Journal of Applied Electrochemistry **33**: 959–967, 2003.

Influence of surface inhomogeneities of boron doped CVD-diamond electrodes on reversible charge transfer reactions☆

D. BECKER and K. JÜTTNER*
Karl-Winnacker-Institute of DECHEMA e.V. Theodor-Heuss-Allee 25, D-60486 Frankfurt am Main, Germany
*(*author for correspondence, e-mail: juettner@dechema.de)*

Received 27 November 2002; accepted in revised form 4 February 2003

Key words: boron doped diamond, diamond electrodes, impedance spectroscopy, partial blocking, reversible charge transfer

Abstract

The electrochemical behaviour of reversible charge transfer reactions on boron doped diamond (BDD) was studied by cyclic voltammetry and electrochemical impedance spectroscopy using rotating disc electrodes under defined convection. Diamond films of 5 μm thickness with doping levels of 200, 3000 and 6000 ppm were prepared by hot filament chemical vapour deposition on niobium substrate. The electrochemical measurements were carried out on BDD electrodes in deaerated 0.5 M Na_2SO_4 + 5 mM $K_3[Fe(CN)_6]/K_4[Fe(CN)_6]$ solution at rotation frequencies $0 < f_{rot} < 4000$ rpm. Comparative measurements were carried out on an active Pt electrode. The BDD electrodes exhibit distinct irreversibilities indicated by a larger peak potential difference in the cyclic voltammograms, lower diffusion limiting current densities and an additional impedance element at high frequencies. Mechanical polishing with carbon fleece and SiC paper strongly affects the irreversible behaviour of the BDD electrodes. The experimental results are explained by a partial blocking of the diamond surface with reversible charge transfer at active sites. The impedance spectra are analysed quantitatively using a transport impedance model for reversible reactions on partially blocked electrode surfaces.

1. Introduction

Boron doped diamond (BDD) electrodes are attractive for many electrochemical applications due to their unique chemical, physical and electrochemical properties [1–6]. This includes chemical inertness, mechanical stability, hardness, and thermal and electrical conductivity. In its undoped form, diamond is an insulator with a band gap of 5.5 eV, whereas p-type or n-type semiconductor and semimetallic behaviour can be achieved by doping with boron, nitrogen and other elements [1, 2, 7, 8]. From the electrochemical point of view, the extremely wide potential window which is observed for water decomposition, makes thin film diamond electrodes attractive for a variety of technical applications in the field of electrosynthesis and electroanalysis. Examples are the formation of peroxodisulfate [9], chlorine [10], hypochloride [11], hydrogen peroxide, ozone and other strongly oxidizing agents [12], which can also act as disinfectants [10]. The outstanding power of diamond electrodes for the oxidation of aliphatic and aromatic compounds, e.g. isopropanol [13, 14], chlorophenols [5, 9, 12, 15], mono- and dicarboxylic acids [16], complex forming agents such as EDTA [17], polyacrylates [12], herbicides and pesticides [15], makes this material promising for the treatment of industrial waste and electrochemical destruction of pollutants [5]. The high reactivity is associated with the formation of hydroxyl radicals which act as intermediates in the oxidation mechanism of organic compounds [12]. In addition, excellent resistance to surface fouling is of great advantage for technical applications [5]. For electroanalysis, diamond electrodes are superior to glassy carbon due to their higher stability, sensitivity and low background currents over a wide potential range [13, 18].

Despite these advantages, there are still a number of properties which are not yet fully understood from a fundamental point of view. For example, kinetic studies of reversible and quasi-reversible redox reactions, such as $Fe(CN)_6^{3-/4-}$, $Ru(NH_3)_6^{3+,2+}$, $IrCl_6^{2-/3-}$, $Fe^{2+/3+}$, $Ce^{3+/4+}$, benzoquinone/hydroquinone, methylviologen etc., show much lower 'electrochemical activity' of CVD diamond electrodes in comparison to glassy carbon or noble metal electrodes [3, 4, 19–30]. In most of the electrochemical studies of diamond electrodes cyclic voltammetry was applied [3, 4, 19, 20, 24–30]. In a few papers characteristic parameters such as 'apparent' rate

☆ This paper was originally presented at the 6th European Symposium on Electrochemical Engineering, Düsseldorf, Germany, September 2002.

constants and diffusion coefficients were determined from the sweep rate and concentration dependence of the voltammograms [19, 20, 23, 27–29]. The influence of surface finishing, mechanical polishing or formation of surface active groups by anodic or cathodic polarization was also investigated [20]. It was found that electrochemical activity depends on sample preparation and the formation of hydrogenated or oxidized surface active groups [1, 2, 5, 10].

Electrochemical impedance spectroscopy has also been applied to characterize the redox behaviour of diamond electrodes [21–23]. Impedance analysis was based on simple RC circuit combinations and the use of constant phase elements [21, 22]. A more advanced semiconductor model was used by Kelly et al. [23] to analyse the impedance of different redox reactions ($Fe(CN)_6^{3-/4-}$, $Fe^{2+/3+}$, $Ce^{3+/4+}$) on diamond films homo-epitaxially grown on single crystal (100) and (110) oriented natural diamond substrates. In this paper, potential dependent surface states energetically distributed within the band gap of p-type diamond were considered to account for the unusual potential dependence of the impedance spectra. In general, the rate constants of the 'outer sphere' redox reactions, determined either by cyclic voltammetry or impedance spectroscopy, were found to be orders of magnitude lower than those found with conventional active noble metal or glassy carbon electrodes.

Here the redox system $K_3[Fe(CN)_6]/K_4[Fe(CN)_6]$ will be studied as a typical example of fast, transport controlled outer-sphere reactions using cyclic voltammetry and impedance spectroscopy under defined convection on rotating disc electrodes and *ex situ* surface analytical techniques. The clear deviation of diamond electrodes from the ideal polarisation behaviour of platinum will be discussed and interpreted in terms of a partial blocking of the diamond electrode surface. An impedance model for transport controlled reactions on partially blocked electrode surfaces will be discussed and applied for the quantitative description of the experimental data and the determination of system specific parameters.

2. Experimental details

Polycrystalline thin film diamond electrodes of 5 μm thickness were prepared by hot filament chemical vapour deposition (HFCVD) on niobium substrate in a hydrogen and methane atmosphere with diboran as the doping gas (concentrations of up to 3.0 vol % [1]). Filament temperatures ranged between 2300 °C and 2800 °C and substrate temperatures between 650 °C and 950 °C. Prior to the deposition process, the polycrystalline niobium substrate was treated by sandblasting to clean and roughen the surface followed by a final cleaning in ultrapure water and seeding with a suspension of diamond powder in alcohol [1]. The diamond samples with boron content of 200, 3000 and 6000 ppm were embedded in Teflon holders and used as rotating disk electrodes (RDE) of 0.5 cm^2 geometrical surface area. The electrochemical measurements were carried out in a three-electrode Duran glass cell at room temperature and rotation frequencies of $0 \leqslant f_{rot} \leqslant 4000$ rpm. For comparison, measurements were also performed on Pt electrodes of the same geometry. An Ag/AgCl (sat. KCl) electrode with a Luggin capillary served as the reference electrode and a platinum sheet of 2 cm^2 geometrical area as the counter-electrode. Aqueous electrolyte solutions with 0.5 M Na_2SO_4 as the supporting electrolyte and 5×10^{-3} M $K_3[Fe(CN)_6]/K_4[Fe(CN)_6]$ as the redox system were prepared from p.a. grade chemicals (Riedel-deHaen). The solutions were deoxygenated by purging with N_2. Zahner IM5d equipment was used for the cyclic voltammetry and the electrochemical impedance measurements in the frequency range of 100 mHz $\leqslant f \leqslant$ 100 kHz with 5 mV a.c. voltage amplitude. The working electrodes (BDD and Pt) were cleaned in an ultrasonic bath (H_2O) and electrochemically activated by cycling between oxygen and hydrogen evolution in 0.5 M Na_2SO_4 solution (100 cycles). To study the influence of mechanical treatment, the diamond electrodes were dry polished with a carbon fleece and wet polished with SiC (1400) paper.

Ex situ surface analytical techniques (SEM, EDX and contact angle measurement) were used to characterize the diamond surface. Deposition of copper from 0.1 M $CuSO_4$ solution at constant overvoltage $\eta = -75$ mV was applied for the decoration of active sites on the diamond surfaces.

3. Results and discussion

3.1. *Polarization curves*

Quasi-steady state polarisation curves in 0.5 M Na_2SO_4 solution were measured in the potential range between oxygen and hydrogen evolution on Pt and BDD electrodes with different boron content (200, 3000, 6000 ppm). Independent of the doping level, the diamond electrodes exhibit a wider potential window of up to 4 V, whereas on platinum the window spans only 2 V (Figure 1). As the boron concentrations used are relatively high, the diamond films can be considered as semimetallic and highly conducting. With Pt it is well known that specific adsorption of reaction intermediates such as OH_{ad} and H_{ad} are involved in the reaction mechanism of oxygen and hydrogen evolution. The fact that on diamond the rates of the two reactions are not affected by the doping level indicates that specific interactions of reaction intermediates are not important or are not involved in the reaction pathway. This is consistent with the interpretation of Comninellis et al. [15, 16, 31], who have shown that the mechanism of oxygen evolution on oxide covered metal electrodes

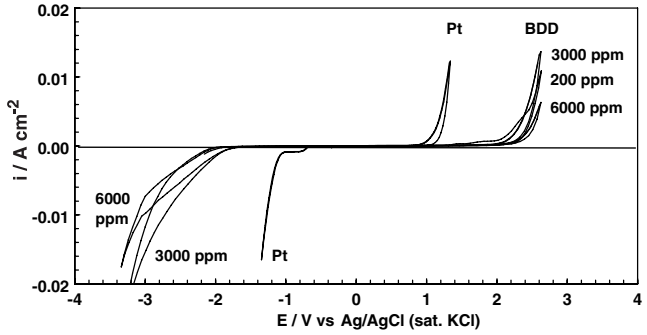

Fig. 1. Steady-state polarization curves of Pt and BDD electrodes in 0.5 M Na_2SO_4 solution purged with N_2. Boron concentrations: 200–3000 ppm; $f_{rot} = 0$ rpm; $|dE/dt| = 5$ mV s^{-1}; $T = 298$ K.

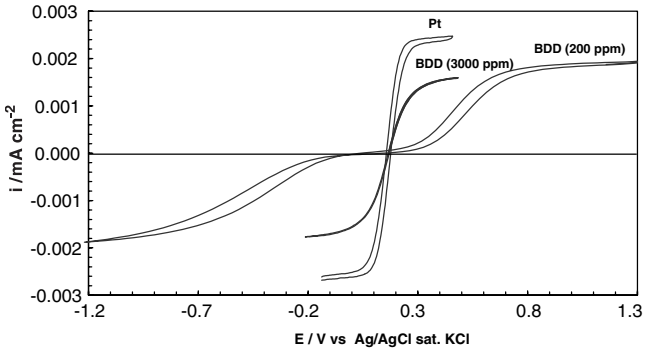

Fig. 3. Cyclic voltammograms of Pt and BDD electrodes in 0.5 M Na_2SO_4 + 5×10^{-3} $K_3[Fe(CN)_6]/K_4[Fe(CN)_6]$ solution purged with N_2. Boron concentrations: 200 ppm, 3000 ppm; $f_{rot} = 1000$ rpm; $|dE/dt| = 100$ mV s^{-1}; $T = 298$ K.

differs significantly from that of diamond electrodes where only short-lived OH radicals form.

3.2. *Cyclic voltammetry*

Figure 2 shows cyclic voltammograms obtained on Pt and BDD electrodes with different boron content in the presence of the redox system 5 mM $K_3[Fe(CN)_6]/K_4[Fe(CN)_6]$ in solution. The voltammogram on Pt exhibits ideal reversible behaviour with a peak potential difference of about 59 mV, whereas the diamond electrodes show strong deviations from reversibility. The peak potential difference increases and the peak currents decrease with decreasing boron content. At the lowest boron level of 200 ppm it can be seen that the anodic and cathodic sweeps are asymmetric. These deviations of the diamond electrodes from ideal behaviour have been described in many papers and were mainly interpreted in terms of a decrease in the reaction rate constant [19]. However, this can only be the case for an 'inner sphere' process, where the reaction mechanism

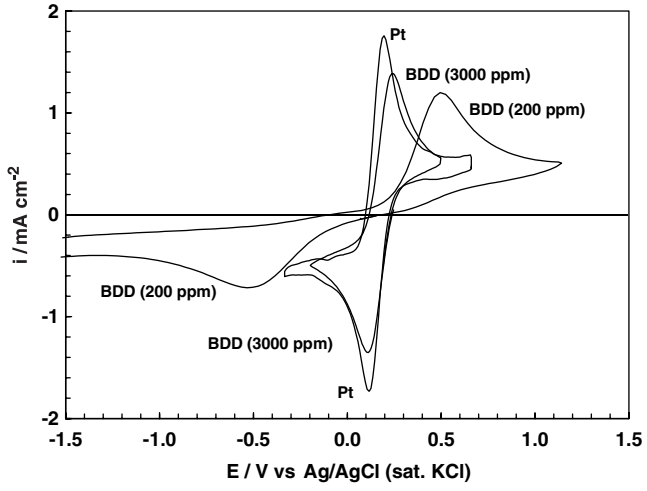

Fig. 2. Cyclic voltammograms of Pt and BDD electrodes in 0.5 M Na_2SO_4 + 5×10^{-3} $K_3[Fe(CN)_6]/K_4[Fe(CN)_6]$ solution purged with N_2. Boron concentrations: 200 ppm, 3000 ppm; $f_{rot} = 0$ rpm; $|dE/dt| = 100$ mV s^{-1}; $T = 298$ K.

and activation energy depend on specific adsorption of reactants or intermediates. This is obviously not the case with the system considered here, which is well known to follow an 'outer sphere' mechanism. Figure 3 shows the polarization curves in the same system but with rotation at a fixed frequency of $f_{rot} = 1000$ rpm. The current density increases strongly, attaining a limiting value, and the polarization curves of the BDD electrodes shift towards higher overvoltage. It is important to note that the limiting current densities of BDD electrodes are significantly lower than on Pt, which cannot be explained in terms of retarded charge transfer kinetics but indicates a strong geometrical blocking of the electrode surface, as will be shown by the following experiments.

3.3. *Electrochemical impedance spectroscopy*

Impedance measurements were carried out on Pt and BDD electrodes with different doping levels in the system 0.5 M Na_2SO_4 + 5×10^{-3} M $K_3[Fe(CN)_6]/K_4[Fe(CN)_6]$. The impedance spectra of Pt at the equilibrium potential ($E = E_o$) are shown in Figure 4(a) for different rotation speed $0 \leqslant f_{rot} \leqslant 4000$ rpm. The impedance spectra over the whole frequency range (100 mHz $\leqslant f \leqslant$ 100 kHz) are typical of a transport controlled redox reaction, the transfer function of which is described by the Nernst impedance:

$$Z_N(j\omega) = R_N \frac{\tanh \sqrt{j\omega/\omega_N}}{\sqrt{j\omega/\omega_N}} \tag{1}$$

with

$$R_N = \frac{2RT\delta_N}{z^2F^2c^sD} \tag{1'a}$$

and

$$\omega_N = \frac{D}{\delta_N^2} \tag{1'b}$$

where δ_N is the thickness of the Nernst diffusion layer, c^s the steady state concentration of the reacting species at

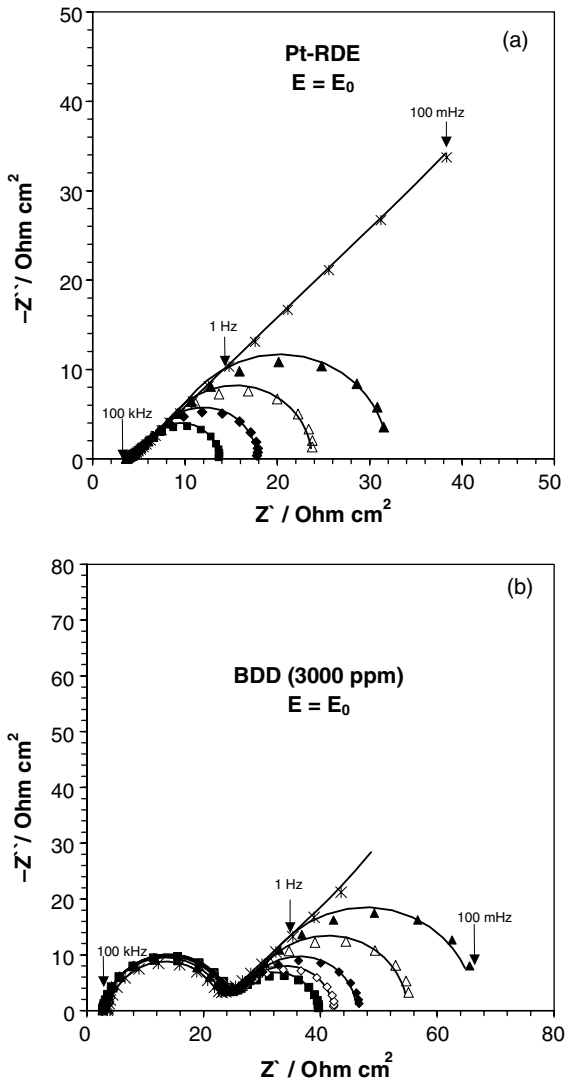

Fig. 4. Rotation dependence of impedance spectra of active Pt (a) and BDD (3000 ppm) (b) electrodes in 0.5 M Na_2SO_4 + 5×10^{-3} $K_3[Fe(CN)_6]/K_4[Fe(CN)_6]$ solution purged with N_2; f_{rot}: (∗) 0, (▲) 500, (△) 1000, (♦) 2000, (◇) 3000 and (■) 4000 rpm; $E = E_o$: $T = 298$ K.

the electrode surface, D the diffusion coefficient, and z, F, R, T have their usual meaning. For rotating disc electrodes, the dependence of δ_N on rotation frequency f_{rot} is described by the Levich equation:

$$\delta_N = \frac{1.6 D^{1/3} \nu^{1/6}}{\sqrt{2\pi f_{rot}}} \tag{2}$$

where ν is the kinematic viscosity of the electrolyte. Without rotation ($f_{rot} = 0$) the diffusion layer thickness tends to infinity, $\delta_N \to \infty$, and with the condition $\omega/\omega_N \gg 1$, Equation 1 leads to an expression denoted as Warburg impedance:

$$Z_W(j\omega) = \frac{2RT}{z^2 F^2 c^s \sqrt{D}} \times \frac{1}{\sqrt{j\omega}} \tag{3}$$

The experimental data in Figure 4(a), including the Warburg line, are well described by Equation 1, which is also evident from the excellent fit results presented as full line curves. The impedance spectra at the BDD electrode(3000 ppm) in Figure 4(b) obtained under identical conditions differ significantly from those of the Pt electrode in Figure 4(a). In addition to the Nernstian diffusion controlled part at lower frequencies, the spectra exhibit a capacitive high frequency (h.f.) element, which shows only weak rotation dependence. This h.f. element appears to be associated with a charge transfer resistance in parallel to a double layer capacitance or constant phase element. However, as will be shown, this assumption does not comply with the overall behaviour of BDD electrodes.

The dependence of the impedance spectra on dc polarization (overvoltage $\eta = E - E_o$) at a fixed rotation ($f_{rot} = 1000$ rpm) is shown in Figure 5(a) and (b) for Pt and BDD, respectively. On increasing the overvoltage η, the impedance of both Pt and BDD expands. Polarization of the electrode generally causes an increase in

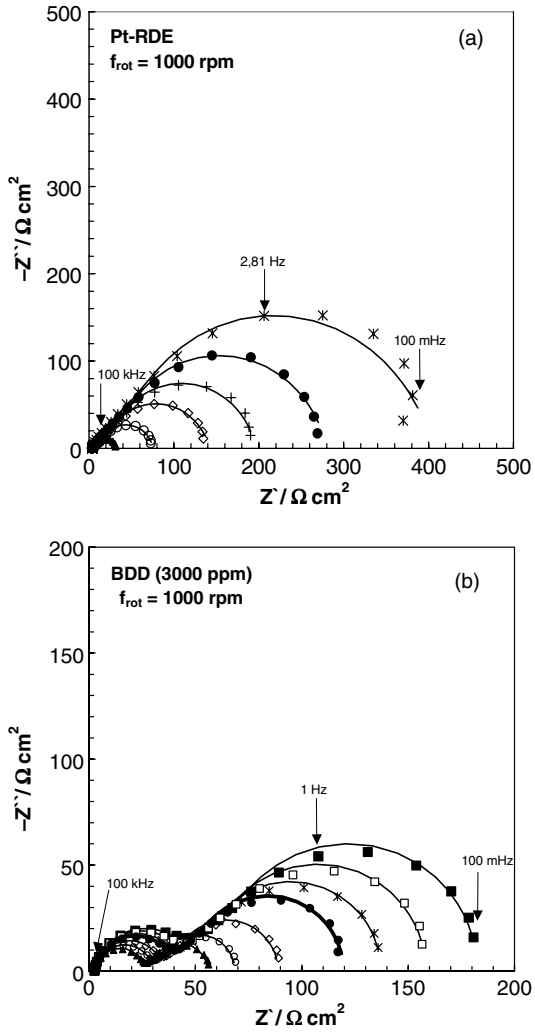

Fig. 5. Overvoltage dependence of impedance spectra of Pt (a) and BDD electrode (b) (3000 ppm) in 0.5 M Na_2SO_4 + 5×10^{-3} M $K_3[Fe(CN)_6]/K_4[Fe(CN)_6]$ solution purged with N_2; η: (■) 100, (□) 90, (∗) 80, (●) 70, (+) 60, (◇) 50, (○) 40 and (▲) 10 mV; $f_{rot} = 1000$ rpm; $T = 298$ K.

reaction rate coupled with a decrease in reactant concentration at the surface. On Pt the increase in the Nernst impedance (Figure 5(a)) is related to the decrease of the concentration c^s, which leads to an increase in R_N according to Equation 1. The same is true for the low frequency part of the BDD electrode (Figure 5(b)) which is to be identified as Nernst impedance. However, the h.f. capacitive element of the BDD electrode also exhibits an increase with the applied overvoltage. Similarly to the discussion of the polarization curves, this does not comply with the interpretation of a charge transfer resistance R_t, which is expected to decrease with increasing overvoltage, according to [32]:

$$R_t = \frac{RT}{z^2F^2k_{sh}} \times \frac{1}{\alpha C_r^s \exp[\alpha\psi] + \beta C_o^s \exp[-\beta\psi]} \qquad (4)$$

where k_{sh} is a standard rate constant, α and $\beta = 1-\alpha$ are the anodic and cathodic charge transfer coefficients, ψ is the potential function $\psi = F(E - E_o)/RT$ and E_o the standard potential of the redox reaction.

An apparent rate constant k_{sh} can be estimated from experimental data at the equilibrium potential ($E = E_o$) where $\psi = 1$ (for $C_r = C_o$). Using an approximate value of $R_t \approx 50\ \Omega\ cm^2$, an approximate value of $k_{sh} \approx 10^{-3}$ cm s^{-1} for $\alpha = 0.5$ and $C_r = C_o = 5 \times 10^{-6}$ mol cm^{-3} is obtained. In the literature $k_{sh} \approx 0.4$ cm s^{-1} is reported [33], which correspond to R_t values as low as $R_t \approx 1\ \Omega\ cm^2$. The results on Pt in Figures 4(a) and 5(a) are in accordance with such low R_t and high k_{sh} values. The unexpected high apparent 'charge transfer resistance' on BDD and its increase with overvoltage η can obviously not be explained in terms of retarded charge transfer kinetics.

3.4. *Effect of surface treatment*

If charge transfer kinetics is not responsible for the observed retardation effects on BDD electrodes, another reason must be found. From the literature it is known that surface treatment can affect the 'electrochemical activity' of diamond electrodes to a large extent [20]. Therefore, we studied the influence of (i) anodic polarization at high current density (1 A cm^{-2}), (ii) dry mechanical treatment with carbon fleece and (iii) wet mechanical treatment with SiC paper on the impedance response of BDD electrodes. Figure 6 shows the influence of surface treatment for a highly blocked BDD electrode in 0.5 M Na_2SO_4 + 5 mM $K_3[Fe(CN)_6]$/$K_4[Fe(CN)_6]$ solution. As can be seen from the decrease in overall impedance in Figure 6(a), the effect of anodic polarization is weak compared to that of carbon fleece treatment, where the impedance order of magnitude decreases from kΩ to a few Ω and finally arrives at the Warburg line of active Pt, as shown in Figure 6(b). However, this activation is not permanent and disappears when the fine carbon particles are washed off the surface. The influence of SiC treatment is depicted in Figure 7, where the h.f. element of the BDD electrode is decreased by a factor of 5.

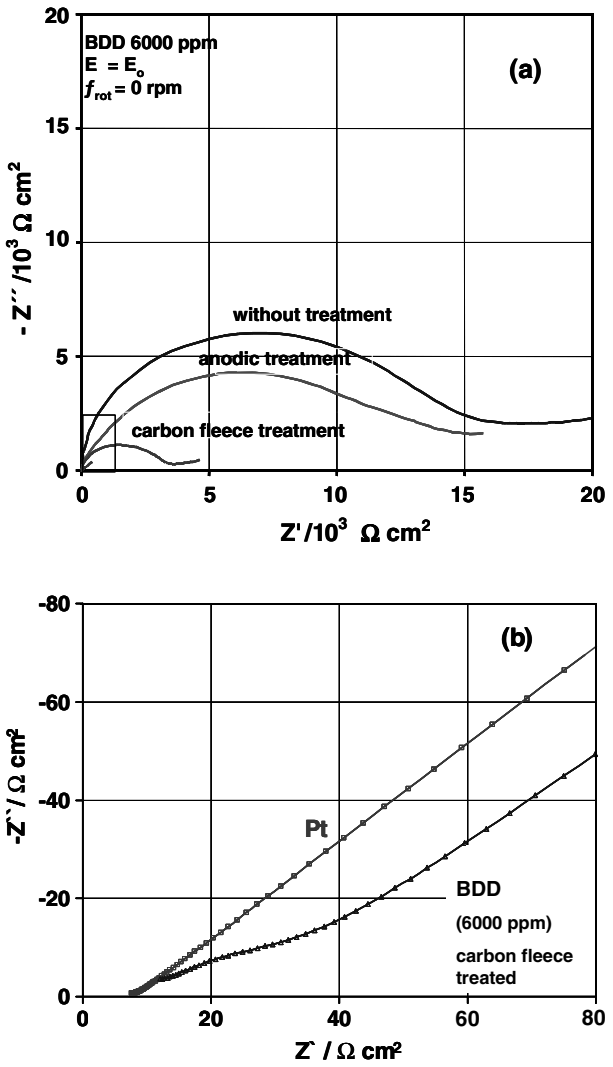

Fig. 6. Influence of surface treatment on impedance spectra of a blocked BDD electrode in 0.5 M Na_2SO_4 + 5×10^{-3} $K_3[Fe(CN)_6]$/$K_4[Fe(CN)_6]$ solution purged with N_2; $E = E_o$; $T = 298$ K; (a) anodic and carbon fleece treatment leading to significant decrease of the impedance; (b) enlarged section of the h.f. part of the impedance of BDD in comparison to active Pt.

These results clearly demonstrate that the h.f. impedance element as a quantitative measure of the 'electrochemical activity' of BDD electrodes is mainly related to the surface properties of the polycrystalline diamond film. It will be shown that the phenomena observed so far can be well explained by assuming that reversible charge transfer on BDD takes place on the restricted area of active sites of a partially blocked electrode surface.

3.5. *Impedance model of partially blocked electrode surfaces*

For transport controlled reactions on a partially blocked electrode surface the decrease of current density is not simply proportional to the active surface area but

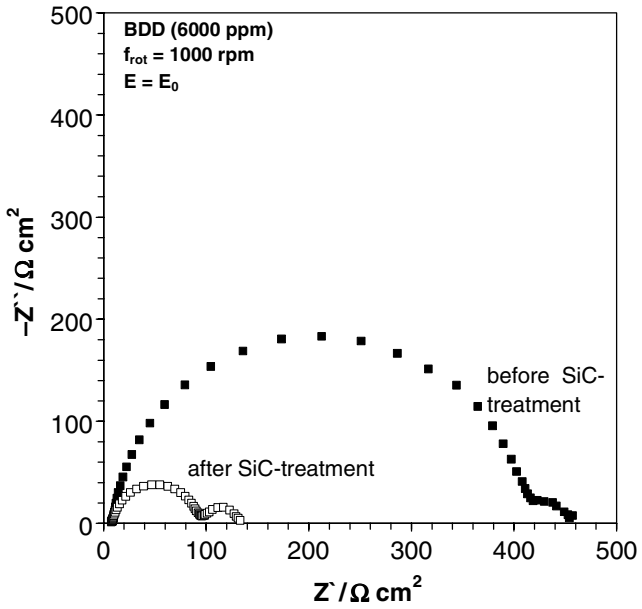

Fig. 7. Influence of surface treatment with SiC (1400) paper on impedance spectra of a blocked BDD electrode.

depends in a complex manner on the number density, size, distance and distribution of active sites. A model approach to describe this effect of partial blocking was first developed by Matsuda et al. [34–36] and later adopted by Schmidt et al. [37, 38] to derive the transfer function of such a system. Figure 8 gives a simplified schematic view of the Matsuda model A pattern. In this model the statistical distribution of active and inactive surface area is approximated by an array of uniform hexagonal patches with circular active sites of radius a in the centre and nearest neighbour distance $2R^*$. The hexagons are replaced by circular patches to reduce the mathematical effort for solving the transport equations in cylindrical coordinates. The degree of surface blocking is described by blocking an index σ, defined as

$$\sigma = \frac{\text{inactive area}}{\text{active area}} = \frac{\pi R^{*2} - \pi a^2}{\pi a^2} \tag{5}$$

If a transport controlled reaction takes place at the electrode surface, a highly nonlinear concentration profile of the electroactive species evolves near the electrode/solution interface. The homogeneous diffusion layer of thickness δ_N with linear concentration gradients and diffusion fluxes perpendicular to the surface is disturbed by an inhomogeneous layer of thickness $\delta_\sigma \leqslant \delta_N$, where concentration gradients and lateral fluxes are emerging in all directions. An approximate Laplace plane solution of the transport equations in terms of average fluxes and boundary conditions exists [37, 38], from which the overall transport impedance can be derived:

$$Z_{tr}(j\omega) = Z_N(j\omega) + \sigma \cdot Z_\sigma(j\omega) \tag{6}$$

This transport impedance, Z_{tr}, consists of the Nernst impedance $Z_N(j\omega)$ and the perturbation term $\sigma \cdot Z_\sigma(j\omega)$, which contains all deviations from the ideal linear diffusion regime arising from the partial blocking of the surface [37].

$$Z_\sigma(j\omega) = R_\sigma \frac{\tanh\sqrt{(j\omega + W)/\omega_\sigma}}{\sqrt{(j\omega + W)/\omega_\sigma}} \tag{7}$$

In Equation 7 the parameters R_σ, ω_σ and W are functions of diffusion and blocking parameters of the non-homogeneous transport layer:

$$R_\sigma = \frac{2RT\delta_\sigma}{z^2F^2c^sD} \tag{8a}$$

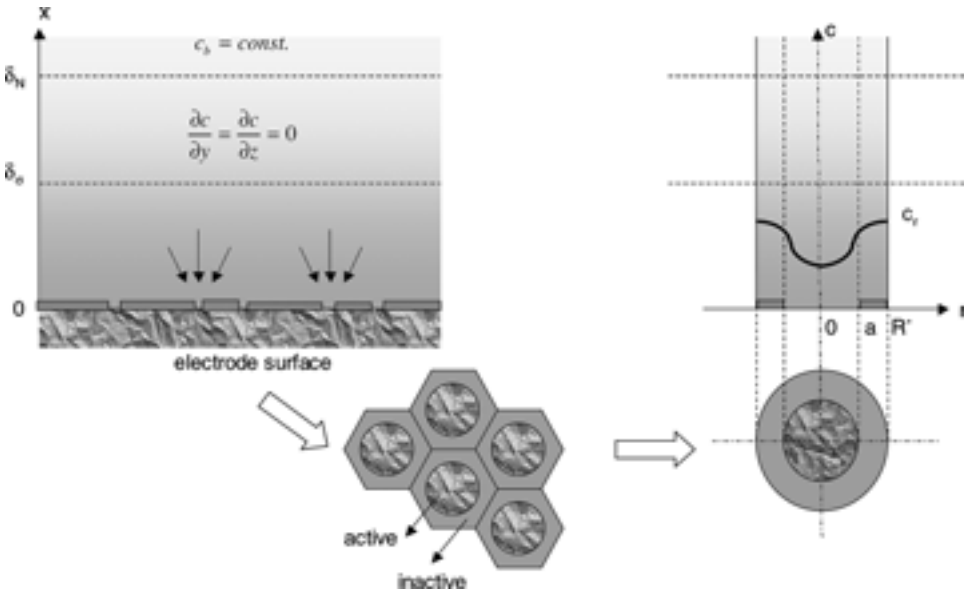

Fig. 8. Schematic diagrams of a partially blocked electrode surface with homogeneous and inhomogeneous diffusion layers developing at the electrolyte interface [34].

and

$$\omega_\sigma = \frac{D}{\delta_\sigma^2} \tag{8b}$$

The mathematical structure of Z_σ is similar to that of Z_N except for the additional parameter W, which is defined as [37]:

$$W = \frac{2D}{R^{*2}} \frac{(1+\sigma)^2}{\sigma} \frac{1}{\ln(1+0.25\sqrt{1+\sigma})} \tag{9}$$

Similarly to ω_N and ω_σ, W can be considered as a characteristic frequency for lateral diffusion between active and inactive regions ($W \approx D/R^{*2}$); if $W = 0$, lateral exchange does not take place.

3.6. *Fit of experimental impedance data*

To fit the experimental data of BDD electrodes using the proposed model, a parallel combination of the transport impedance Z_{tr} and a double layer capacitance C_{dl} was used in series with an electrolyte resistance R_{el}, as shown in Figure 9. The double layer capacity on Pt was found to be $C_{dl} \approx 20\ \mu F\ cm^{-2}$, whereas on BDD a value of $C_{dl} \approx 7\ \mu F\ cm^{-2}$ was found. The adjustable parameters of the transport impedance are R_N, ω_N, R_σ, ω_σ, σ and W. It should be noted that σ and R_σ form a product in Equation 6 and cannot be obtained independently. Therefore, in the first run of the fitting procedure the parameters R_N and ω_N were determined while in the second run the parameters R_σ and ω_σ were fixed to these values assuming that $\delta_\sigma \approx \delta_N$. By this means approximate values of σ and W could be determined bearing in mind that they are affected with a certain error. The quality of the fit results is very good as can be seen from the full line curves in Figures 4 and 5, representing the model simulation.

The fit parameters ω_N, R_σ, σ and W obtained from the impedance data of BDD in Figures 4(b) and 5(b) are plotted in Figures 10, 11 and 12 as a function of rotation frequency f_{rot} and overvoltage η. As expected from Equations 1′ and 2, the fit parameter ω_N is found to be linearly dependent on rotation frequency f_{rot} at fixed potential $E = E_o$ (Figure 10(a)) and independent of the applied overvoltage η at constant rotation frequency $f_{rot} = 1000$ rpm (Figure 10(b)). The diffusion coefficient D calculated from $\omega_N \approx 2.2\ s^{-1}$ (Figure 10(b)) is found

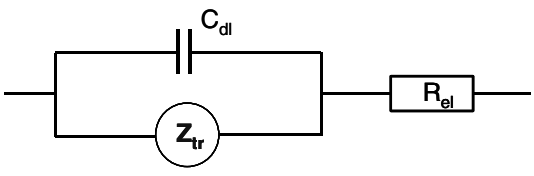

Fig. 9. Equivalent circuit to fit the experimental impedance data of Figures 4(b) and 5(b) by the transport impedance Z_{tr} (Equation 6). C_{dl} = double layer capacitance; R_{el} = electrolyte resistance.

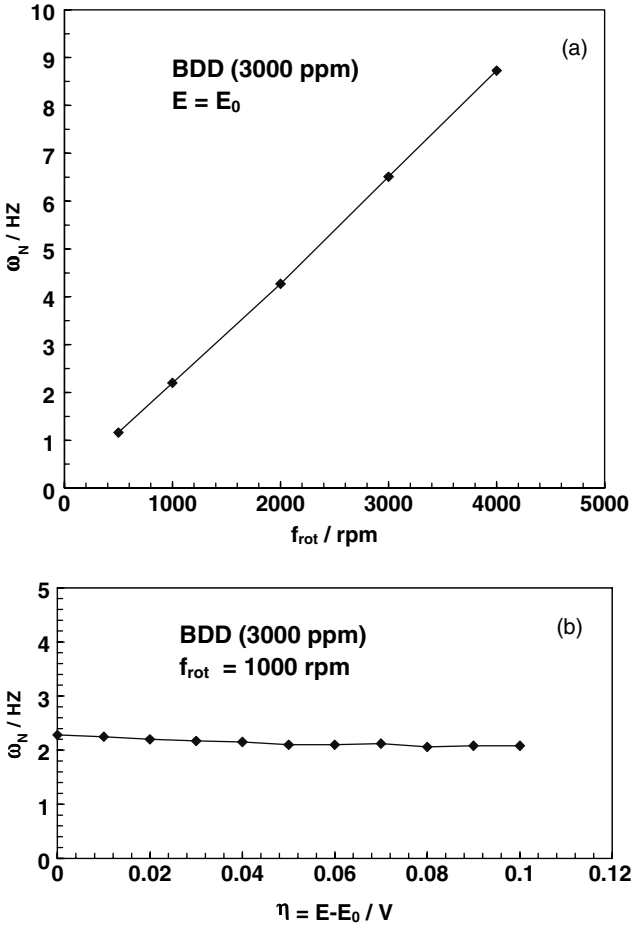

Fig. 10. Fit parameter ω_N as a function of rotation frequency (a) and overvoltage (b) obtained from the experimental data in Figures 4(b) and 5(b).

to be in the order of $D = 4 \times 10^{-6}\ cm^2\ s^{-1}$, which is in good agreement with literature data [33].

The fit parameters R_σ ($\approx R_N$), σ and W are plotted in Figures 11 and 12. The parameter R_σ ($\approx R_N$) decreases with increasing rotation frequency as predicted from the dependence of δ_σ ($\approx \delta_N$) on f_{rot} in Equations1′ and 2. On the other hand, the increase in R_σ with increasing

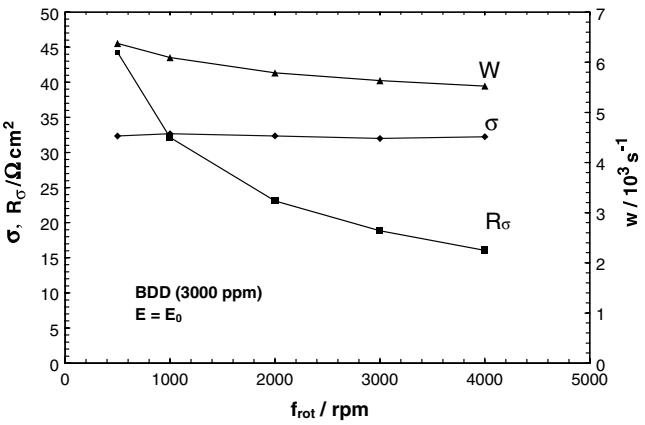

Fig. 11. Fit parameters R_σ, σ and W as a function of rotation frequency obtained from the results in Figure 4(b).

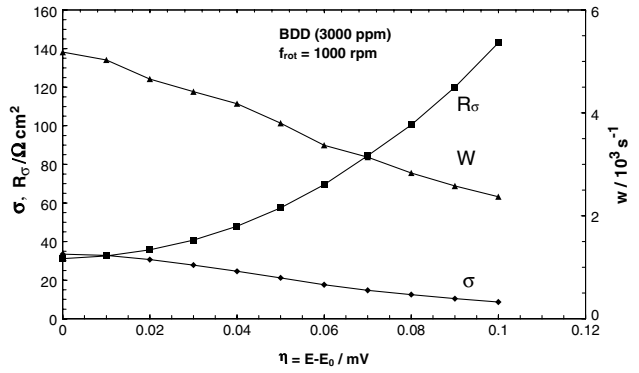

Fig. 12. Fit parameters R_σ, σ and W as a function of overvoltage obtained from the results in Figure 5(b).

overvoltage in Figure 12 is due to the decrease in surface concentration c^s in Equation 8. At equilibrium potential $E = E_o$, the degree of surface blocking σ and the characteristic frequency W are not substantially affected by the rotation frequency f_{rot} as depicted in Figure 11. From these data, the mean distance of active sites ($2R^* \approx 5.5$ μm) can be calculated using Equation (9). This distance is in the order of the diffusion layer thickness δ_N at $f_{rot} = 1000$ rpm, which explains the observed lower limiting diffusion current density of BDD electrodes in Figure 3. The effect of partial blocking on diffusion limited current density becomes remarkable only when the distance of active sites gets in the order of the diffusion layer thickness as described, for example, by Landsberg and Thiele [39]. From the experiments, the number of active sites N^* is estimated to be of the order of $N^* \approx 1/\pi R^{*2} \approx 10^6$ cm^{-2}.

Although the parameters σ and W are almost independent of the rotation frequency f_{rot}, a distinct overvoltage dependence is found, as shown in Figure 12. On changing η from 0 to 100 mV, the parameters σ and W decrease by a factor of about one half. However, this corresponds only to a small variation of the structure sensitive parameter $2R^* \approx 5.5$–5.6 μm, which is in good agreement with the Cu decoration experiments. The micrographs in Figure 13 show the BDD (3000 ppm) surface after electrodeposition of a certain amount of Cu from 0.1 M $CuSO_4$ solution. The mean distance of the copper particles (white spots) deposited on the active sites is close to the value found for $2R^*$ from the fit results.

The observed overvoltage dependence of σ and W may be also due to strong changes in the steady state concentration profile in the inhomogeneous transport layer. On decreasing the steady state surface concentration c^s, the concentration gradients are getting steeper and lateral fluxes between active and inactive areas are strongly enhanced.

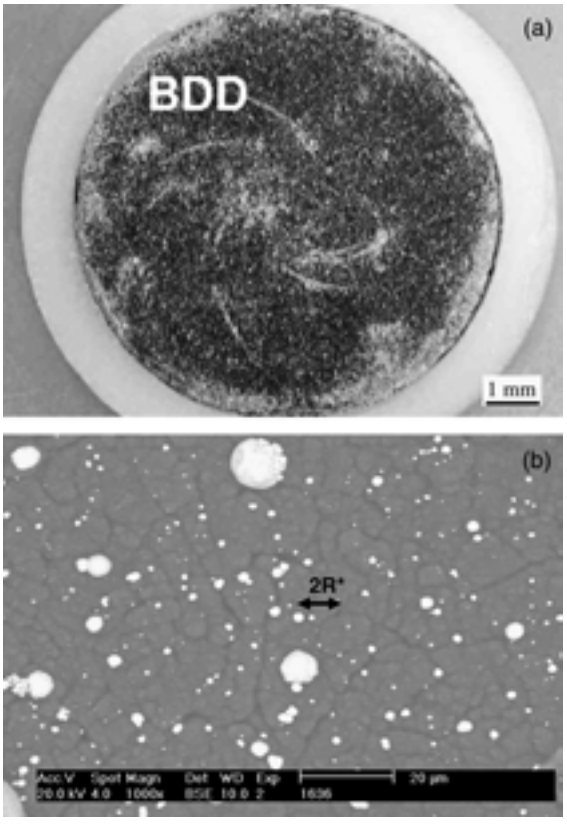

Fig. 13. Decoration of active sites (white spots) with copper deposits on BDD (3000 ppm). Distance of active sites $2R^*$ (↔) obtained from fit of impedance data; (a) microscopic image; (b) BSE (backscattered electrons) image.

4. Conclusions

The experimental results show strong deviations of reversible charge transfer for the typical 'outer sphere' redox reaction $K_3[Fe(CN)_6]/K_4[Fe(CN)_6]$ on BDD electrodes compared to Pt. These deviations are reflected by a larger peak potential difference and shift of the peak potentials in cyclic voltammograms, lower limiting current densities under forced convection at the RDE and the appearance of an additional capacitive element in the impedance spectra at higher frequencies. These findings indicating lower 'electrochemical activity' of the BDD electrodes need not be interpreted in terms of a decrease in the rate constant of the 'outer sphere' reaction as has been the case in previous studies. The observed strong dependence on surface treatment (prepolarization and mechanical treatment) and the rotation and polarization dependence of the impedance spectra favour the assumption of a geometrical surface blocking rather than changes in the charge transfer kinetics. This was demonstrated by fitting the experimental data with a model for transport controlled reactions on a partially blocked electrode surface. The model describes the experimental results fairly well and the fit parameters are in accordance with physical data of the system. The distance of active sites ($2R^* \approx 6$ μm) and the number density ($N^* \approx 1 \times 10^6$ cm^{-2}) calculated from fit parameters are also in good agreement with the data of direct surface analysis. In the light of these results, the astonishing activation of a highly blocked BDD electrode by mechanical treatment with carbon fleece can be understood as the temporary formation of a thin carbon

film interconnecting the active sites and promoting the electron transfer on the whole surface area. The reasons for the partial blocking on the diamond surface are not yet clear. In homogeneous composition of the diamond leading to singularities at the surface with enhanced electron density and conductivity (e.g., sp^2 carbon phases or agglomerations of the boron dopant) may be responsible for the observed phenomena.

Acknowledgements

The authors acknowledge financial support by the Deutsche Forschungsgemeinschaft DFG (JU 201-8). We also thank our project partners M. Fryda, L. Schäfer and I. Troester, Fraunhofer Institut für Schicht und Oberflächentechnik, IST Braunschweig/Germany, for providing us with the boron doped diamond electrodes.

References

1. I. Tröster, L. Schäfer and M. Fryda, *New Diamond and Frontier Carbon Technol.* **12** (2002) 89.
2. M. Fryda, A. Dietz, T. Matthee, L. Schäfer and C.-P. Klages, *Nachr. Chem. Tech. Lab.* **45** (1997) 379.
3. G.M. Swain and R. Ramesham, *Anal. Chem.* **65** (1993) 345.
4. G.M. Swain, *Adv. Mater.* **6** (1994) 388.
5. A. Fujishima, C. Terashima, K. Honda, B.V. Sarada and T.N. Rao, *New Diamond and Frontier Carbon Technol.* **12** (2002) 73.
6. M. Fryda, L. Schäfer and I. Tröster, *in* S.G. Pandalai (Ed.), *Recent Res. Devel. Electrochem.* **4**, Transworld Research Network (2001) 85.
7. C.-P. Klages and L. Schäfer, *in* B. Dischler and C. Wild (Eds), 'Low-Pressure Synthetic Diamond', Springer Series in Materials Processing (Springer Verlag, Berlin, Heidelberg, 1998), pp. 85–101.
8. I. Yagi, K. Tsunozaki, A. Fujishima, B. Ohtani and K. Uosaki, *J. Electrochem. Soc.* **149** (2002) E1.
9. P.A. Michaud, E. Mahe, W. Haenni, A. Perret and Ch. Comninellis, *Electrochem. Solid-State Lett.* **3** (2000) 77.
10. W. Haenni, J. Gobet, A. Perret, L. Pupunat, P. Rychen, Ch. Comninellis and B. Correa, *New Diamond and Frontier Carbon Technol.* **12** (2002) 83.
11. H.-J. Förster, W. Thiele, D. Fassler and K. Günther, *New Diamond and Frontier Carbon Technol.* **12** (2002) 99.
12. L. Gheradini, P.A. Michaud, M. Panizza and Ch. Comninellis, *J. Electrochem. Soc.* **148** (2001) D78.
13. T. Yano, D.A. Tryk, K. Hashimoto and A. Fujishima, *J. Electrochem. Soc.* **145** (1998) 1870.
14. K. Patel, K. Hashimoto and A. Fujishima, *Denki Kagaku* **60** (1992) 659.
15. B. Boye, P.-A. Michaud, B. Marselli, M.M. Dieng, E. Brillas and Ch. Comninellis, *New Diamond and Frontier Carbon Technol.* **12** (2002) 63.
16. D. Gandini, E. Mahe, P.A. Michaud, W. Haenni, A. Perret and Ch. Comninellis, *J. Appl. Electrochem.* **30** (2000) 1345.
17. J. Wurm, *New Diamond and Frontier Carbon Technol.* **12** (2002) 107.
18. C. Reuben, E. Galun, H. Cohen, R. Tenne, R. Kalish, Y. Muraki, K. Hashimoto, A. Fujishima, J.M. Butler and C. Levy-Clement, *J. Electroanal. Chem.* **396** (1995) 233.
19. S. Ferro and A. Battisti, *Electrochim. Acta* **47** (2002) 1641.
20. F. Marken, C.A. Paddon and D. Asogan, *Electrochem. Commun.* **4** (2002) 62.
21. Y.V. Pleskov, V.P. Varnin, I.G. Teremetskaya and A.V. Churikov, *J. Electrochem. Soc.* **144** (1997) 175.
22. J. van de Lagemaat, G.Z. Cao, G. Janssen, D. Vanmaekelbergh and J.J. Kelly, *Electrochem. Soc. Proc.* **95-21** (2000) 103.
23. J. van de Lagemaat, D. Vanmaekelbergh and J.J. Kelly, *J. Electroanal. Chem.* **475** (1999) 139.
24. C.H. Goeting, F. Jones, J.S. Foord, J.C. Eklund, F. Marken, R.G. Compton, P.R. Chalker and C. Johnston, *J. Electroanal. Chem.* **442** (1998) 207.
25. C.H. Goeting, F. Marken, A. Gutiérrez-Sosa, R.G. Compton and J.S. Foord, *New Diamond and Frontier Carbon Technol.* **3** (1999) 207.
26. Y.V. Pleskov, Y.E. Evstefeeva, M.D. Krotova and A.V. Laptev, *Electrochim. Acta* **44** (1999) 3361.
27. Y. Maeda, K. Sato, R. Ramaraj, T.N. Rao, D.A. Tryk and A. Fujishima, *Electrochim. Acta* **44** (1999) 3441.
28. M.C. Granger, M. Witek, J. Xu, J. Wang, M. Hupert, A. Hanks, M.D. Koppang, J.E. Butler, G. Lucazeau, M. Mermoux, J.W. Strojek and G.M. Swain, *Anal. Chem.* **72** (2000) 3793.
29. G. Pastor-Moreno and D.J. Riley, *Electrochem. Commun.* **4** (2002) 218.
30. K.B. Holt, G. Sabin, R. Compton, J.S. Foord and F. Marken, *Electroanal.* **14** (2002) 797.
31. G. Foti, D. Gandini, C. Comninellis, A. Perret and W. Haenni, *Electrochem. Solid-State Lett.* **2** (1999) 228.
32. M. Sluyters-Rehbach and J.H. Sluyters, *in* A.J. Bard (Ed.), 'Electroanalytic Chemistry', Vol. 4, (Marcel Dekker, New York, 1970) pp. 1–121.
33. M. Stiebel and K. Jüttner, *J. Electroanal. Chem.* **290** (1990) 163.
34. T. Gueshi, K. Tokuda and H. Matsuda, *J. Electroanal. Chem.* **89** (1978) 247.
35. T. Gueshi, K. Tokuda and H. Matsuda, *J. Electroanal. Chem.* **101** (1979) 29.
36. K. Tokuda, T. Gueshi and H. Matsuda, *J. Electroanal. Chem.* **102** (1979) 41.
37. J. Hitzig, J. Titz, K. Jüttner, W.J. Lorenz and E. Schmidt, *Electrochim. Acta* **29** (1984) 287.
38. E. Schmidt, J. Hitzig, J. Titz, K. Jüttner and W.J. Lorenz, *Electrochim. Acta* **31** (1986) 1041.
39. R. Landsberg and R. Thiele, *Electrochim. Acta* **11** (1966) 1243.